Facile Synthesis of Micrometer-sized Hierarchical Porous Si@C Anodes for High-Performance Lithium-Ion Batteries

Shuai Xu,[†] x,[††] Xin Zhang, [†] Julia Zhao[††] and Xiaodong Hou[,†]*

[†] Institute for Energy Studies, University of North Dakota, Grand Forks, ND, 58202, United States

[††] Department of Chemistry, University of North Dakota, Grand Forks, ND, 58202, United States

*E-mail: xiaodong.hou@und.edu

Abstract:

Extensive studies have been conducted to determine if replacing graphite anodes with silicon is feasible since silicon possesses a high capacity and is an abundant resource; however, Si anodes suffer significant volume changes during cycling, which pulverizes its structure and subsequently causes rapid capacity fading. We used SiO_2 nanoparticles ($nSiO_2$) and low-cost coal-derived humic acid as a feedstock to synthesize high performance Si-C anodes for Li-ion Batteries through spray drying, calcination, and magnesiothermic reductions. Our Si-C anodes features micrometer-sized porous Si coated with a graphitized carbon shell (mpSi@C). The hierarchical graphitized carbon shell and porous silicon structure relieve the mechanical stress of the Si phase upon cycling, which stabilizes the structure. This mpSi@C composite design allows for a high initial discharge capacity of 2199.9 mAh g^{-1} at 0.1 A g^{-1} and a cycling performance of 68% capacity retention after 100 cycles at 1.0 A g^{-1}. The multipoint contact between the Si anode and C structure allows for a remarkable performance rate of 566.3 mAh g^{-1} at 5.0 A g^{-1}.

Keywords: humic acid, porous silicon, magnesiothermic reduction, hierarchical structure, lithium-ion batteries

Introduction

Silicon is a promising next-generation anode for lithium-ion batteries (LIBs) due to the increasing demand for electronics and energy storage systems with high energy densities and long cycling lives.[1-3] Silicon anodes can possess a capacity of 4,200 mAh g^{-1}, which is more than ten times higher than currently used graphite anodes. Silicon resources are widely available and abundant; however, its high capacity is offset by its drastic volume change during lithiation and delithiation, approximately 400%, V/V_o, which pulverizes the Si particles and lowers the electrical contacts with current collectors.[4, 5] The side reactions between Si and the electrolyte form the solid-

electrolyte interphase (SEI), which is vulnerable to repeated cycling and consumes the electrolyte, resulting in a thick SEI and deteriorated Li^+ transport. These problems all lead to low cycling efficiency and rapid capacity loss.

Many approaches have been proposed to address these problems. Si nanolization is a widely accepted effective solution since nanometer-sized diameter (D < 150 nm) Si survives cycling without pulverization[6, 7]. Nano-Si also decreases the diffusion length of lithium ions[8-10]; therefore, numerous types of nano-Si, including nanowires,[11] nanotubes[12, 13], and nanospheres[14], have been synthesized to improve performance. Nevertheless, these nano-Si structures have an enlarged surface area, which enhances the side reactions between Si and the electrolyte. The synthesis of nano-Si is a complicated and exact process, making nano-Si expensive and less practical for massive production.[15] Porous silicon has clusters with a large quantity of nano-Si particles and voids, yielding some unique advantages compared to nano-silicon alone, including smaller surface area, lower production cost, and better thermodynamic stability.[5, 16] The voids in the porous structure can freely accommodate silicon expansion and contraction during the lithiation/delithiation process.[5, 17, 18] These attributes have encouraged researchers to explore the porous silicon anode synthesis processes for LIBs.[19-22] The Magnesiothermic Reduction (MR reaction) of SiO_2 is a promising method to synthesize porous silicon due to its much lower reaction temperature and controllable porosity.[23-25] Nanosized-porous and microsized-porous Si structures synthesized by MR reactions have been reported; [16, 26] however, a defect of the nanoporous structure is its significant electrolyte consumption due to its large surface area, leading to the low ICE observed in nano-Si. Microsized porous Si has a higher ICE due to its smaller surface area, whereas, its mechanical strength is limited due to its much larger size than that of nano-porous Si, making it easier to fracture during cycling.[26]

Graphene coatings have been proposed as an ideal approach to support porous Si structures and limit the side reactions between Si and the electrolyte due to excellent resilience and high conductivity;[27-29] however, previously manufactured graphene coatings are sophisticated, need catalysts, and endure harsh conditions during the synthesis process, limiting production substantially. Low-cost graphene synthesized from a low-cost feedstock, such as coal, is highly desirable and may be a promising approach.[30-33]

Coal is classified as low-rank, medium-rank, or high-rank according to the degree of coalification.[34] Humic acid (HA), the primary organic component of low-rank coal (lignite) is derived from peat and has a molecule weight range from several hundred to millions.[35] HA is a dark brown powder where two-thirds of the carbon atoms in its molecule are sp^2 bonded. The rest of the atoms exist primarily in carboxyl groups and hydroxyl groups (Figure 1a). The unique structure of HA is a promising precursor for high-quality graphene synthesis;[31, 36] however, these approaches require harsh synthesis conditions, including expensive catalysts, and high temperature and pressure, which incurs a prohibitive cost for mass production.

Scheme 1. Schematic illustration of the synthetic process of the mpSi@C composite.

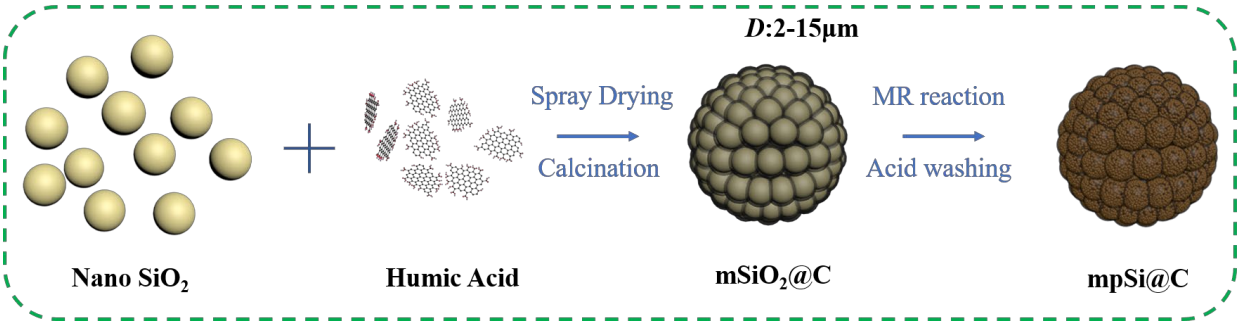

In this work, we have introduced SiO_2 nanoparticles ($nSiO_2$) and a feedstock of low-cost coal-derived HA to synthesize micrometer-sized porous Si coated with a graphitized carbon shell (mpSi@C) through spray drying, calcination, and MR reactions (Scheme 1). The obtained mpSi@C composite possesses a microsized hierarchical graphitized carbon structure that encapsulates the nanoporous Si (npSi) to effectively release the mechanical stress of Si anode upon lithiation. Detailed electrochemical testing and characterizations were performed to determine the effectiveness of the design.

Experimental Section

1. Synthesis of the $mSiO_2$@C composite

A quantity of 3.5 g HA, extracted and purified from North Dakota lignite, was dissolved in 30 mL of D.I. water with ammonium (1.0 mL, 28%–30%, LabChem, USA). The mixture was stirred at 200 rpms for 1 hour, followed by the addition of 10.0 g SiO_2 nanoparticles (500nm) and 0.45 g P123 as a surfactant. The result was stirred vigorously for 2 hours then spray-dried at an inlet

temperature of 200 ℃. The powder obtained from spray drying, $mSiO_2$@HA, was sintered at 300 ℃ for 2 hours, then at 800 ℃ for 5 hours in a high-purity Ar atmosphere to produce $mSiO_2$@C.

2. Synthesis of the mpSi@C composite

A total of 0.81 g $mSiO_2$@C powder containing 0.7 g SiO_2 was completely mixed with 0.6g Magnesium powder (325 mesh, Sigma Aldrich, USA) and 4.0 g NaCl powder (Sigma Ultra, USA) in a glovebox. The mixture was sealed in a stainless steel tube then heated to 700 ℃ for 5 hours at a heating rate of 4℃/min under an Ar atmosphere. The resulting powder was washed in sequence with HCl solution (10%, A.C.S) for 2 hours and an HF solution (5%, Sigma Aldrich, USA) for 20 minutes to remove impurities. The mpSi@C composite was obtained after D.I. water washing and vacuum drying.

3. Materials characterization

Powder X-ray diffraction (XRD) was performed on an X-ray diffractometer (Smartlab, Rigaku) using Cu Kα radiation at a scan rate of 2°/minute, from 10°–80°. Field-mission scanning electron microscopy (FEI Quanta 650 FEG SEM) was used to analyze the particle morphology. The Raman spectra were collected with a Raman Spectrometer (HORIBA, 532 nm, 1800 grating). The mpSi@G carbon content was analyzed with a carbon analyzer (TOC-V, SHIMADZU) that uses an SSM 5000A module for solid samples.

4. Electrochemical measurements

The electrode paste was prepared by mixing the mpSi@G composite, a conductive agent (Carbon nanotube), and CMC (Carboxymethyl Cellulose) at a mass ratio of 90: 4: 6 in D.I. water. The paste was then laminated onto copper foil and dried overnight at 80 ℃ in a vacuum oven. The coated foil was punched into disk electrodes with diameters of 14 mm. Coin-type cell (CR2032) assembly was performed in an Ar-filled glovebox using the mpSi@G electrode as the working electrode, lithium foil as the counter electrode, a Celgard 2400 membrane as the separator, and 1.2 M LiPF6 in EC/DMC/EMC = 1/1/1 (wt%) with 10 wt% FEC as the electrolyte. The cells were evaluated at 25 ℃ with galvanostatic charge-discharge testing between 0.01 V and 1.5 V (vs. Li/Li^+) on a Neware Battery testing system (CT-4008, Neware Technology Limited, Shenzhen. China). The current densities and specific capacities were calculated based on the mass of the active materials in the working electrode. Electrochemical impedance spectroscopy (EIS) and cyclic voltammetry

(CV) were performed on a Gamry interface 1010E electrochemical workstation (Gamry Instruments, USA). CV measurements were conducted in the voltage range of 0.01-2.0 V at 0.1 mV S^{-1}. EIS measurements were performed at an AC voltage amplitude of 10 mV and a frequency of 1 MHz to 0.1 Hz.

Results and discussion

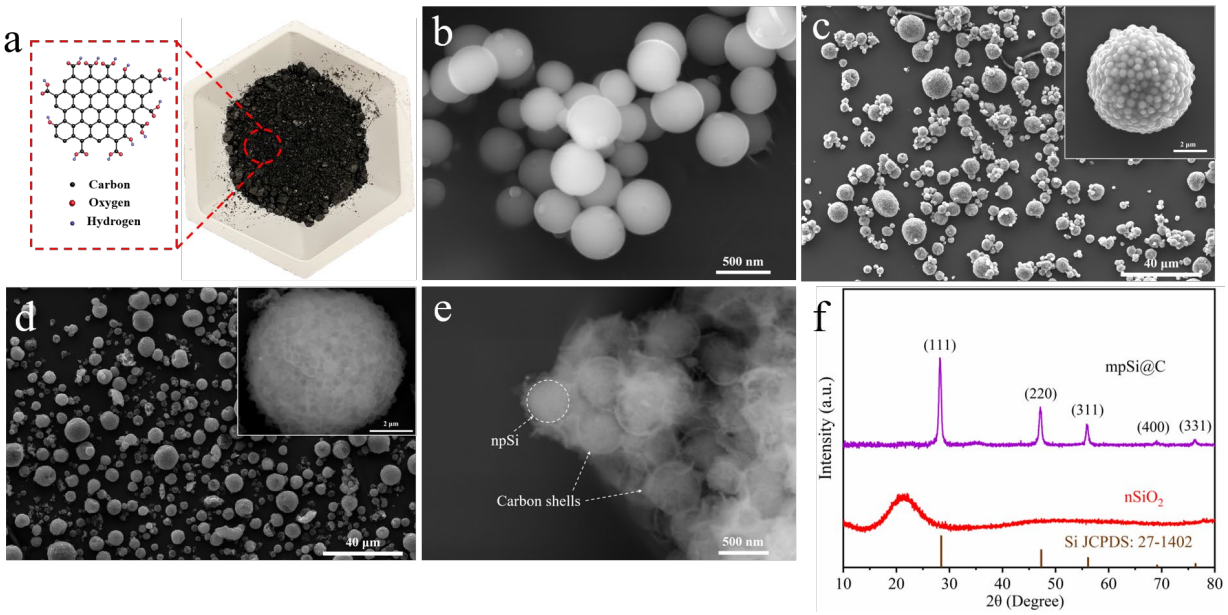

Figure 1. (a) HA powder and its idealized molecular structure. SEM images of (b) $nSiO_2$ particles, (c) $mSiO_2$@C particles and a magnified inset image, (d) mpSi@C particles and a magnified BSE inset image, (e) a broken mpSi@C particle, and (f) XRD patterns of $nSiO_2$ powder and the mpSi@C composite.

We used $nSiO_2$ powder that consists of nano spherical particles with an average particle size of 500 nm (Figure 1b). Micrometer-sized SiO_2 coated with graphitized carbon ($mSiO_2$@C) was obtained by spray drying and calcination. Spray drying is a mature technologyfor the massive production of microsized particles.[37] An $nSiO_2$ and HA slurry was atomized into mist during spray drying, consisting of many small slurry droplets. The droplets contained a water solvent that evaporates instantaneously under the high-temperature inlet gas, leaving the $mSiO_2$@HA particles. The subsequent calcination converted $mSiO_2$@HA to $mSiO_2$@C with a carbon content of 13.6%. Most of the $mSiO_2$@C particles were spherical, with particle sizes ranging from 2-15 μm (Figure 1c). The magnified SEM image of an $mSiO_2$@C particle (Figure 1c inset) reveals the distribution

of $nSiO_2$ and carbon, where $nSiO_2$ constitutes the main body of the $mSiO_2$@C particle and is connected and coated by carbon material. The $nSiO_2$ particles react with the Mg vapor from the sublimation of Mg powder at high temperature, forming an Si and MgO composite, as shown in the magnesiothermic reaction (MR reaction):[23, 25]

$$SiO_2 + 2Mg = Si + 2MgO$$

HCl washing and HF etching romoved the MgO and unreacted SiO_2, leaving the mpSi@C particles (Figure 1d) with a shape identical to the $mSiO_2$@C particles. The magnified BSE inset image in Figure 1d indicates that solid $nSiO_2$ particles were converted to a porous structure. This finding was supported by the high-resolution SEM image of a broken mpSi@C particle (Figure 1e), revealing nanoporous Si particles and surrounding carbon shells. This hierarchical structure is conducive to good electrochemical performance during cycling since the carbon network inside the mpSi@C particles increases its conductivity, while the outer carbon coating prevents side reactions between Si and the electrolytes. The XRD patterns in Figure 1f confirm the proposed phase change in Scheme 1. The broad peak located at 2θ = 15 ~25° indicates the amorphous nature of the $nSiO_2$ powder. A high purity mpSi@C composite was collected after the synthesis process, with all peaks belonging to the Si phase. The Raman spectroscopy analysis was conducted (Figure 2), revealing a significant G-band (1585 cm^{-1}) that demonstrates the highly graphitic nature of the carbon in the mpSi@C composite, while the considerable D-band (1350 cm^{-1}) indicates many defects that will facilitate Li-ion transport through the micrometer-sized particles.

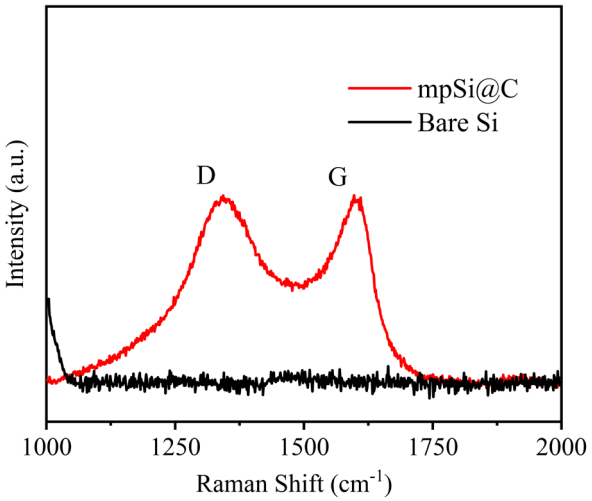

Figure 2. Raman spectra of bare Si and the mpSi@C composites.

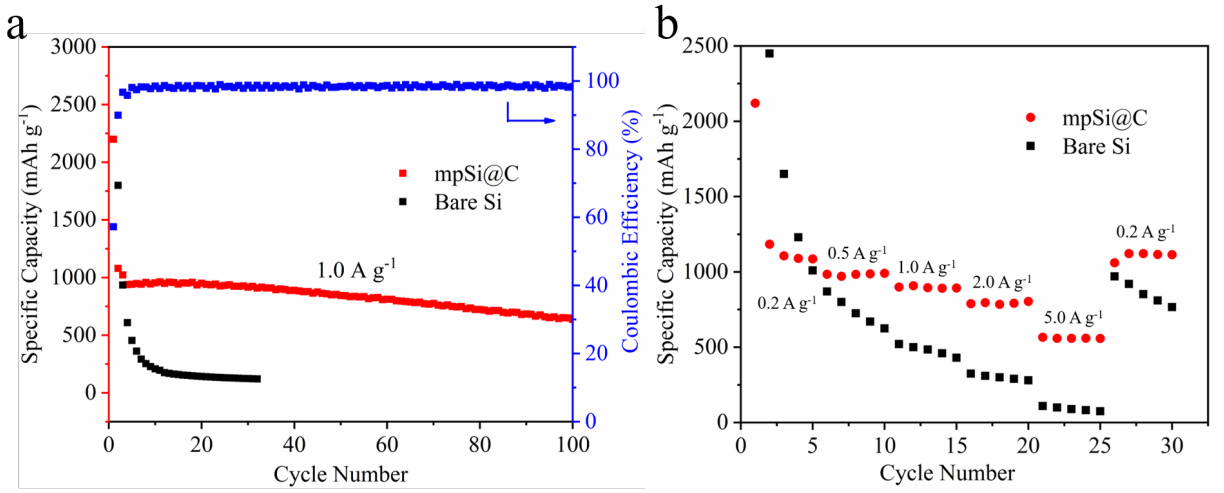

Figure 3. (a) Cycling performance and coulombic efficiency of mpSi@C and the cycling performance of mpSi@C at 1.0 A g^{-1}. (b) Rate capabilities of bare-Si and mpSi@C electrodes.

Cycling and rate testing results (Figure 3) reveal a remarkable electrochemical improvement compared to bare Si material. The mpSi@C composite presents a high initial discharge capacity of 2199.9 mAh g^{-1} at 0.1 A g^{-1} (Figure 3a), which is lower than the bare Si capacity of 3310.4 mAh g^{-1}; however, due to the benefits from the well-designed hierarchical structure, the mpSi@C composite presents considerable cycling performance at 1.0 A g^{-1}, with a 68% capacity retention after 100 cycles. The capacity of bare Si dropped significantly, below 200 mAh g^{-1} in 10 cycles. The rate capability testing of the mpSi@C composite and bare Si were conducted at a series of current densities. The mpSi@C composite delivered reversible capacities of 1183.7, 984.6, 899.2, 789.1, and 566.3 mAh g^{-1} at current densities of 0.2, 0.5, 1.0, 2.0, 5.0 A g^{-1}, respectively (Figure 3b). When the current density was decreased to 0.2 A g^{-1}, the capacity nearly recovered to its original value of 1121.3 mAh g^{-1}. The capacity of bare Si dropped significantly with the increase in current density and could not recover its capacity when the current density returned to 0.2 A g^{-1}. The considerable cycling and rate performance of the mpSi@C composite are contributed to the Si and carbon structure in at least three ways: 1) the nanoporous Si structure could accommodate the volume change of Si during lithiation and delithiation without breaking the surrounding carbon shell, 2) the highly graphitized carbon structure presented high electrical conductivity for charge transfer through the whole micrometer-sized particle, creating a high rate performance, and 3) the outer carbon coating effectively prevented the reactions between the embedded Si and electrolytes, limiting the growth of the SEI film.

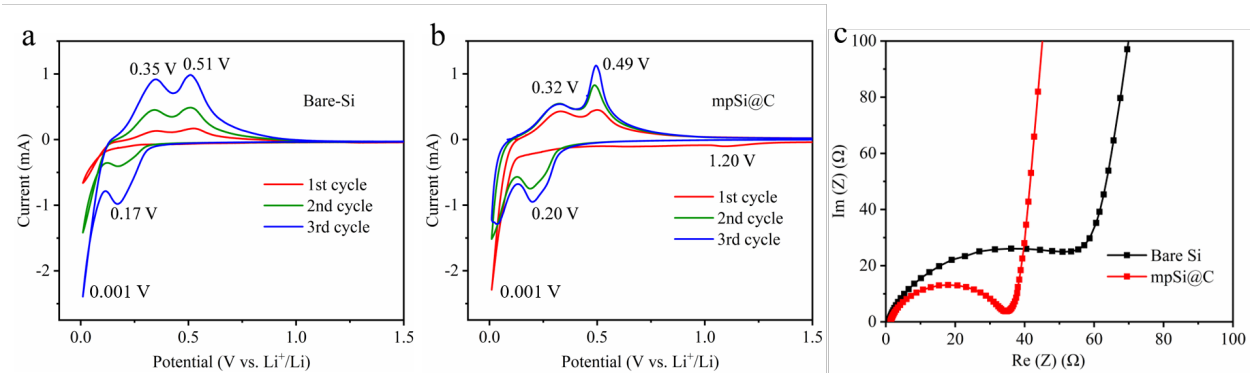

Figure 4. (a) Cyclic voltammetry curves of bare-Si and (b) mpSi@C at a scan rate of 0.1 mV S^{-1} for the first three cycles. (c) Nyquist plots of bare-Si and mpSi@C electrodes before cycling.

The CV curves in Figures 4a and 4b describe the first three cycles of the bare-Si and mpSi@C composite at a scan rate of 0.1 mV S^{-1}. The initial mpSi@C cathodic scan revealed a broad peak at 1.2 V that should be attributed to the SEI film formation between the carbon shell and the electrolyte. The reductive peak in the range of 0.01-0.2V corresponds to the Si phase lithiation in bare Si and mpSi@C. The two oxidation peaks at 0.35 and 0.51 V for bare Si and 0.32 and 0.49 V for mpSi@C can be attributed to the removal of lithium from the as-formed Li_xSi alloy. The peak current increased gradually from the first to third cycle as more Si participated in the alloying process. The difference between the redox peak potential (ΔE_p) for mpSi@C at 0.001 V and 0.49 V was smaller than that of the bare Si at 0.001 V and 0.51 V, indicating a faster current response in mpSi@C due to the hierarchical Si and carbon structure, which facilitates electron transfer and Li-ion transport during potential scanning. These results are supported by the Nyquist results (Figure 4c) obtained from electrochemical impedance spectroscopy (EIS) analysis. Nyquist plots for both bare Si and mpSi@C exhibit one depressed semicircle in the high-frequency range, corresponding to charge-transfer resistance and an inclined line in the low-frequency region associated with Li^+ diffusion.[38] Apparently, the mpSi@C composite possesses a much smaller charge-transfer resistance than bare Si due to its much smaller semicircle.

Conclusion

In summary, we have demonstrated a feasible approach to creating an mpSi@C composite using SiO_2 nanoparticles and a feedstock of coal-derived HA. The rationally designed carbon structure hinders the side reactions between the electrolyte and the embedded nanoporous Si, significantly improving the conductivity of the composite. The mpSi@C composite presents a remarkable

cycling performance of 68% capacity retention after 100 cycles and rate capabilities of 566.3 mAh g^{-1} at 5.0 A g^{-1}. This work provides a new and practical approach for improving Si anode performance for use in LIBs.

Acknowledgments

We acknowledge the support of Jennifer Weidman, Congjun Wang, and Christopher Matranga from NETL for collecting the Raman spectra. National Energy Technology Laboratory through NETL-Penn State University Coalition for Fossil Energy Research (UCFER contract number DE-FE0026825) is greatly appreciated.

Conflict of Interest

The authors declare no conflict of interest.

References

1. Armand, M.; Tarascon, J.-M. Building Better Batteries. *nature* **2008,** *451* (7179), 652.
2. Park, C.-M.; Kim, J.-H.; Kim, H.; Sohn, H.-J. Li-Alloy Based Anode Materials for Li Secondary Batteries. *Chemical Society Reviews* **2010,** *39* (8), 3115-3141.
3. Ma, D.; Cao, Z.; Hu, A. Si-Based Anode Materials for Li-Ion Batteries: A Mini Review. *Nano-Micro Letters* **2014,** *6* (4), 347-358.
4. Shi, F.; Song, Z.; Ross, P. N.; Somorjai, G. A.; Ritchie, R. O.; Komvopoulos, K. Failure Mechanisms of Single-Crystal Silicon Electrodes in Lithium-Ion Batteries. *Nat. Commun.* **2016,** *7*, 11886.
5. Ge, M.; Fang, X.; Rong, J.; Zhou, C. Review of Porous Silicon Preparation and Its Application for Lithium-Ion Battery Anodes. *Nanotechnology* **2013,** *24* (42), 422001.
6. Liu, X. H.; Zhong, L.; Huang, S.; Mao, S. X.; Zhu, T.; Huang, J. Y. Size-Dependent Fracture of Silicon Nanoparticles During Lithiation. *ACS nano* **2012,** *6* (2), 1522-1531.
7. Gu, M.; He, Y.; Zheng, J.; Wang, C. Nanoscale Silicon as Anode for Li-Ion Batteries: The Fundamentals, Promises, and Challenges. *Nano Energy* **2015,** *17*, 366-383.
8. Wang, B.; Li, X.; Qiu, T.; Luo, B.; Ning, J.; Li, J.; Zhang, X.; Liang, M.; Zhi, L. High Volumetric Capacity Silicon-Based Lithium Battery Anodes by Nanoscale System Engineering. *Nano letters* **2013,** *13* (11), 5578-5584.

9. Kasavajjula, U.; Wang, C.; Appleby, A. J. Nano-and Bulk-Silicon-Based Insertion Anodes for Lithium-Ion Secondary Cells. *Journal of power sources* **2007,** *163* (2), 1003-1039.

10. Szczech, J. R.; Jin, S. Nanostructured Silicon for High Capacity Lithium Battery Anodes. *Energy Environ. Sci.* **2011,** *4* (1), 56-72.

11. Chan, C. K.; Peng, H.; Liu, G.; McIlwrath, K.; Zhang, X. F.; Huggins, R. A.; Cui, Y. High-Performance Lithium Battery Anodes Using Silicon Nanowires. *Nature nanotechnology* **2008,** *3* (1), 31-35.

12. Hu, J.; Bando, Y.; Liu, Z.; Zhan, J.; Golberg, D.; Sekiguchi, T. Synthesis of Crystalline Silicon Tubular Nanostructures with Zns Nanowires as Removable Templates. *Angewandte Chemie* **2004,** *116* (1), 65-68.

13. Park, M.-H.; Kim, M. G.; Joo, J.; Kim, K.; Kim, J.; Ahn, S.; Cui, Y.; Cho, J. Silicon Nanotube Battery Anodes. *Nano letters* **2009,** *9* (11), 3844-3847.

14. Liu, N.; Wu, H.; McDowell, M. T.; Yao, Y.; Wang, C.; Cui, Y. A Yolk-Shell Design for Stabilized and Scalable Li-Ion Battery Alloy Anodes. *Nano letters* **2012,** *12* (6), 3315-3321.

15. Rehman, W. U.; Wang, H.; Manj, R. Z. A.; Luo, W.; Yang, J. When Silicon Materials Meet Natural Sources: Opportunities and Challenges for Low‐Cost Lithium Storage. *Small* **2019**, 1904508.

16. Jia, H.; Zheng, J.; Song, J.; Luo, L.; Yi, R.; Estevez, L.; Zhao, W.; Patel, R.; Li, X.; Zhang, J.-G. A Novel Approach to Synthesize Micrometer-Sized Porous Silicon as a High Performance Anode for Lithium-Ion Batteries. *Nano Energy* **2018,** *50*, 589-597.

17. Ge, M.; Lu, Y.; Ercius, P.; Rong, J.; Fang, X.; Mecklenburg, M.; Zhou, C. Large-Scale Fabrication, 3d Tomography, and Lithium-Ion Battery Application of Porous Silicon. *Nano letters* **2014,** *14* (1), 261-268.

18. Xiao, Q.; Gu, M.; Yang, H.; Li, B.; Zhang, C.; Liu, Y.; Liu, F.; Dai, F.; Yang, L.; Liu, Z. Inward Lithium-Ion Breathing of Hierarchically Porous Silicon Anodes. *Nature communications* **2015,** *6* (1), 1-8.

19. Ge, M.; Rong, J.; Fang, X.; Zhang, A.; Lu, Y.; Zhou, C. Scalable Preparation of Porous Silicon Nanoparticles and Their Application for Lithium-Ion Battery Anodes. *Nano Research* **2013,** *6* (3), 174-181.

20. Lee, M. J.; Lee, K.; Lim, J.; Li, M.; Noda, S.; Kwon, S. J.; DeMattia, B.; Lee, B.; Lee, S. W. Outstanding Low‐Temperature Performance of Structure‐Controlled Graphene Anode

Based on Surface‐Controlled Charge Storage Mechanism. *Advanced Functional Materials* **2021**, 2009397.

21. Tian, H.; Tian, H.; Yang, W.; Zhang, F.; Yang, W.; Zhang, Q.; Wang, Y.; Liu, J.; Silva, S. R. P.; Liu, H. Stable Hollow‐Structured Silicon Suboxide‐Based Anodes toward High‐Performance Lithium‐Ion Batteries. *Advanced Functional Materials* **2021**, 2101796.

22. Liu, N.; Lu, Z.; Zhao, J.; McDowell, M. T.; Lee, H.-W.; Zhao, W.; Cui, Y. A Pomegranate-Inspired Nanoscale Design for Large-Volume-Change Lithium Battery Anodes. *Nature nanotechnology* **2014,** *9* (3), 187-192.

23. Entwistle, J.; Rennie, A.; Patwardhan, S. A Review of Magnesiothermic Reduction of Silica to Porous Silicon for Lithium-Ion Battery Applications and Beyond. *Journal of Materials Chemistry A* **2018,** *6* (38), 18344-18356.

24. Bao, Z.; Weatherspoon, M. R.; Shian, S.; Cai, Y.; Graham, P. D.; Allan, S. M.; Ahmad, G.; Dickerson, M. B.; Church, B. C.; Kang, Z. Chemical Reduction of Three-Dimensional Silica Micro-Assemblies into Microporous Silicon Replicas. *Nature* **2007,** *446* (7132), 172-175.

25. Shi, L.; Wang, W.; Wang, A.; Yuan, K.; Yang, Y. Understanding the Impact Mechanism of the Thermal Effect on the Porous Silicon Anode Material Preparation Via Magnesiothermic Reduction. *Journal of Alloys and Compounds* **2016,** *661*, 27-37.

26. Wang, W.; Favors, Z.; Ionescu, R.; Ye, R.; Bay, H. H.; Ozkan, M.; Ozkan, C. S. Monodisperse Porous Silicon Spheres as Anode Materials for Lithium Ion Batteries. *Scientific reports* **2015,** *5*, 8781.

27. Kucinskis, G.; Bajars, G.; Kleperis, J. Graphene in Lithium Ion Battery Cathode Materials: A Review. *J. Power Sources* **2013,** *240*, 66-79.

28. Li, H.; Zhou, H. Enhancing the Performances of Li-Ion Batteries by Carbon-Coating: Present and Future. *Chem. Commun.* **2012,** *48* (9), 1201-1217.

29. Li, Y.; Yan, K.; Lee, H.-W.; Lu, Z.; Liu, N.; Cui, Y. Growth of Conformal Graphene Cages on Micrometre-Sized Silicon Particles as Stable Battery Anodes. *Nature Energy* **2016,** *1* (2), 1-9.

30. Wu, J.; Cao, Y.; Zhao, H.; Mao, J.; Guo, Z. The Critical Role of Carbon in Marrying Silicon and Graphite Anodes for High‐Energy Lithium‐Ion Batteries. *Carbon Energy* **2019,** *1* (1), 57-76.

31. Powell, C.; Beall, G. W. Graphene Oxide and Graphene from Low Grade Coal: Synthesis, Characterization and Applications. *Curr. Opin. Colloid Interface Sci.* **2015,** *20* (5-6), 362-366.

32. Choi, S. H.; Nam, G.; Chae, S.; Kim, D.; Kim, N.; Kim, W. S.; Ma, J.; Sung, J.; Han, S. M.; Ko, M. Robust Pitch on Silicon Nanolayer–Embedded Graphite for Suppressing Undesirable Volume Expansion. *Adv. Energy Mater.* **2019,** *9* (4), 1803121.

33. Beall, G. W.; Duraia, E.-S. M.; Yu, Q.; Liu, Z. Single Crystalline Graphene Synthesized by Thermal Annealing of Humic Acid over Copper Foils. *Physica E: Low-dimensional Systems and Nanostructures* **2014,** *56*, 331-336.

34. Parr, S. W. *The Classification of Coal*; University of Illinois at Urbana Champaign, College of Engineering …: 1928.

35. Stevenson, F. J. *Humus Chemistry: Genesis, Composition, Reactions*. John Wiley & Sons: **1994**.

36. El-shazly, M. D.; Henderson, B.; Beall, G. W. Reduced Humic Acid Nanosheets and Its Uses as Nanofiller. *J. Phys. Chem. Solids* **2015,** *85*, 86-90.

37. Vehring, R. Pharmaceutical Particle Engineering Via Spray Drying. *Pharmaceutical research* **2008,** *25* (5), 999-1022.

38. Cui, J.; Cui, Y.; Li, S.; Sun, H.; Wen, Z.; Sun, J. Microsized Porous SiO_X@ C Composites Synthesized through Aluminothermic Reduction from Rice Husks and Used as Anode for Lithium-Ion Batteries. *ACS applied materials & interfaces* **2016,** *8* (44), 30239-30247.